
[View Journal Online](#)
[View Article Online](#)

Spectroscopic and molecular docking elucidation to binding characteristics of bovine serum albumin with bupropion an aminoketone-medication for nicotine addiction

 Manjushree Makegowda  and Revanasiddappa Hosakere Doddarevanna *

 Department of Chemistry, University of Mysore, Manasagangothri, Mysuru 570 006, Karnataka, India
 mmanjushreem@gmail.com (M. M.), hdrevasiddappa@yahoo.com (R. H. D.).

 * Corresponding author at: Department of Chemistry, University of Mysore, Manasagangothri, Mysuru 570 006, Karnataka, India.
 Tel: +91.821.2419669 Fax: +91.821.2419363 e-mail: hdrevasiddappa@yahoo.com (R.H. Doddarevanna).

RESEARCH ARTICLE

ABSTRACT



doi: 10.5155/eurjchem.10.2.146-155.1845

Received: 08 March 2019

Received in revised form: 29 April 2019

Accepted: 04 May 2019

Published online: 30 June 2019

Printed: 30 June 2019

KEYWORDS

 Metal ions
 Bupropion
 Spectroscopy
 Molecular docking
 Bovine serum albumin
 Drug-protein interaction

One of the highly soluble protein presents in circulatory system of bovine body is bovine serum albumin (BSA). Bupropion hydrochloride (BRN) served to treat prime smoking cessation and disorder due to depressive. BRN binding to BSA was studied by molecular docking and lots of spectroscopic (UV-vis, emission, synchronous, 3D fluorescence, CD and FT-IR) methods at pH = 7.40. Static quenching with strong binding was obtained for BSA-BRN system by forming complex. Secondary structures, conformations and microenvironments of BSA were altered after BRN interaction. Distance between BRN and BSA was also achieved. Biologically active metal ions (Cu^{2+} , Ca^{2+} , Mg^{2+} , Fe^{2+} and Zn^{2+}) were also influenced on the BSA-BRN complex. Bonds of hydrogen and Van der Waals were major binding forces to stabilize BSA-BRN complex at site I (IIA) of BSA. Hence, binding of BRN to transport protein (BSA) is of prominent importance and these findings could be helpful for BRN pharmacology and potential clinical research.

 Cite this: *Eur. J. Chem.* 2019, 10(2), 146-155

 Journal website: www.eurjchem.com

1. Introduction

Bupropion hydrochloride (Figure 1(A)) is an aminoketone class related to phenylethylamines, named as (\pm)-1-(3-chlorophenyl)-2-[(1, 1-dimethylethyl)amino]-1-propanone hydrochloride. Moreover, BRN was chemically incoherent to existing antidepressant agents, tricyclic and tetracyclics. BRN is benefited to treat distinct mental/mood (seasonal affective and bipolar) disorders, depression, facilitates to prohibit suicidal thoughts/attempts and smoking cessation. The often BRN side effects are, dizziness, trouble sleeping, vomiting, sore throat, dry mouth, nausea, allergic reaction (rash and itching/swelling) [1,2].

Broadly, biological performances are influenced by extensive binding of ligand and protein [3-6]. Drug-protein binding mechanism information is expected to examine specific pharmacokinetic (excretion, metabolism, distribution and interaction with particular tissues) and pharmacodynamic (therapeutic impact) properties of drugs. BSA (Figure 1(B)) is the utmost extensively evaluated serum albumin with three (I-III) structural domains. Each domain formulated by two sub-domains nominally A and B. It arranged of 582 amino acids

with Trp134 (on exterior) and Trp 213 (hydrophobic pocket) [7-9].

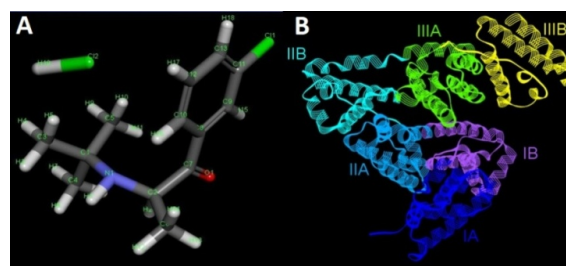


Figure 1. 3D structure of (A) BRN and (B) BSA by discovery studio visualization.

Based on reported literature [10], the interactive binding between bupropion and human serum albumin compared with the present work on bupropion binding to bovine serum albumin shows many differences notably the studied BSA has 2 Trp but HSA has single, also their sequential amino acids are dissimilar and the conducted experimental conditions at

varied temperatures are absolutely differs. The obtained fluorescence, thermodynamic and binding variables are entirely different. The determined metal ions effect on binding interaction also varied. Bupropion binds to different amino acids of BSA at sufficient distances is also distinct from HSA binding.

Plasma proteins recognized to bind across 95% medications. However, the elaborated BSA binding to BRN mechanism was examined by applying many spectroscopic and further by docking applications. Metal ions effects on BSA-BRN binding were also inspected.

2. Experimental

2.1. Materials

BRN; HPLC ($\geq 98\%$), BSA; agarose gel electrophoresis ($\geq 99\%$), warfarin analytical standard; ibuprofen; GC ($\geq 98\%$), digitoxin; HPLC ($\geq 92\%$), trace metal basis: copper (II) chloride ($\geq 97\%$), calcium carbonate ($\geq 99.995\%$), magnesium chloride hexahydrate ($\geq 99.995\%$), tetrahydrate of iron (II) chloride (99.997%), zinc chloride ($\geq 99.999\%$) were retrieved from Sigma-Aldrich (USA). Analytical standard form was took part for all the furthest solvents, chemicals and reagents.

2.2. Analytical procedures

Stock solutions: a concentration of 1.0×10^{-3} mol/L was prepared for BRN, metal ions and three site markers where BSA at 1.0×10^{-4} mol/L in Tris buffer (Tris of 0.05 M, NaCl of 0.15 M and dilute HCl). Throughout every experiment making employed double-distilled water, pH of 7.40 was maintained and applied the background buffer correction.

2.3. UV-visible absorption spectroscopy

Absorption spectrum in UV-vis region (200-300 nm) was recorded on Beckman Coulter "Life Sciences" DU 730 UV-visible Spectrophotometer (U.S.A) furnished with a path length 10 mm of quartz cell for BSA (1.8×10^{-6} mol/L) with BRN (0 to 3.0×10^{-6} mol/L) increasing concentrations at 297 K.

2.4. Fluorescence emission spectroscopy

F-4600 spectrophotometer fluorescence Hitachi (Japan) was exercised to perform all fluorescence measurements equipped with Xenon lamp 150W. Thermostat was circulated to preserve the desirable temperatures. Emission fluorescence spectrum was recorded at 287, 297 and 307 K temperatures in 290 to 420 nm. In addition, excitation/emission slits widths were set at 10/10 nm and excitation wavelength kept at 295 nm. BSA at 1.8×10^{-6} mol/L concentration with BRN added from 0 to 3.0×10^{-6} mol/L. By using Equation (1), correction was made on received fluorescence intensity values from inner filter effect.

$$F_{cor} = F_{obs} \times e^{(A_{ex} + A_{em})/2} \quad (1)$$

where, F_{obs} and F_{cor} are the observed and corrected intensities fluorescence, respectively. At wavelengths of excitation/emission, absorption measurements were done for BRN as A_{ex} and A_{em} , respectively [11].

2.5. Infrared spectroscopy

FT-IR spectral recording of BSA and BSA-BRN system were done on Perkin Elmer FT-IR spectrometer Spectrum Two (USA) furnished with accessory, detector and beam splitter as ATR (attenuated total reflection) germanium as OptKBr,

deuterated-triglycinesulphate and KBr, respectively. A resolution of 4 cm^{-1} and an around of 90 scans was employed to $1500\text{-}1700 \text{ cm}^{-1}$ regions at 297 K. Both the BSA and BRN concentrations were kept at 6.0×10^{-6} mol/L with the spectral subtraction from buffer pH = 7.40. Secondary structure compositions were performed on software of 64 Bit ORIGINPRO 9.0 to region of amide I.

2.6. Circular dichroism (CD) spectropolarimetry

BSA CD measurements with and without BRN were achieved at 297 K in the range 200-240 nm on JascoJ-815 circular dichroism spectropolarimeter (Japan) with scanning speed 100 nm/min and band width 1.00 nm. The concentration of BRN used was 20 folds higher than BSA concentration (6.0×10^{-6} mol/L) and cell length of 10 mm was employed. Calculations of secondary structure were executed on (bestsel.elte.hu/) online BeStSel software.

2.7. Determinations of energy transfer

Energy transfer between BSA and BRN was calculated from overlapping of fluorescence and UV-vis absorption spectrum of BSA and BRN, respectively at 297 K in the wavelength range of 295-400 nm. Concentrations of BSA and BRN were kept at 6.0×10^{-6} mol/L.

2.8. Molecular docking

With the assistance of Lamarckian genetic algorithm, molecular docking studies were performed by utilizing Autodock Tools 1.5.6 and Autodock 4.2. The structures of BSA and BRN were downloaded from Protein Data Bank (PDB id: 3V03) and PubChem (CID 62884), respectively. The geometry optimization and energy minimization was done for both BSA and BRN with the help of GROMOS96 (43B1) force field present in Swiss-Pdb Viewer software and Marvin View software, respectively. Addition of polar hydrogens, salvation criterion, Kollman charges and subsequent removal of water molecules to BSA were utilized as input for Auto Dock Tools. The non-polar hydrogens and their rotatable bonds were merged for BRN. 2016 Biovia Discovery Studio software was applied to visualize the derived docking results. By employing the Autogrid 4.2 a grid maps of dimension of $60 \times 60 \times 60$ along three coordinates with grid space of 0.375 \AA were defined separately for each binding sites I, II and III. x , y and z coordinates for each binding sites were prepared according to the respective amino acids present in BSA. Approximately individuals of 150, energy evaluations of 250,000 and generations of 27,000 were implemented for each run out of 80 runs with tolerance 2.0 \AA . With help of deviation to root mean square, cluster analysis were performed by keeping mutation of 0.02, crossover weights of 0.8, and elitism 1.0 for docked results.

2.9. Synchronous fluorescence spectroscopy

BSA (1.8×10^{-6} mol/L) synchronous fluorescence spectra with different concentrations of BRN (0 to 3.0×10^{-6} mol/L) were note down for Tyr and Trp by setting $\Delta\lambda$ values at 15 and 60 nm, respectively. The recorded wavelength range was 245 to 320 nm at 297 K.

2.10. Three-dimensional (3D) fluorescence spectroscopy

The wavelengths of excitation and emission were designated to 200-380 and 250-500 nm, respectively for the analysis of three-dimensional fluorescence of free BSA and BSA-BRN complex at 297 K. The ratio of 1:40; 3.0×10^{-6} ; 90×10^{-6} mol/L was maintained for BSA to BRN concentrations.

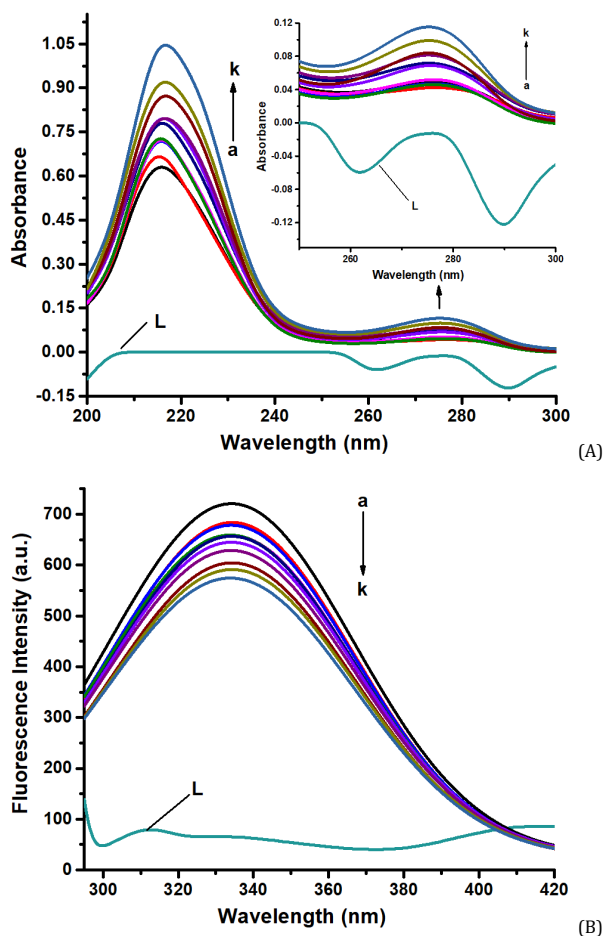


Figure 2. Spectra of (A) UV-vis absorption and (B) fluorescence emission of BSA (1.8×10^{-6} mol/L) in various amounts of BRN (0 to 3.0×10^{-6} mol/L), curve L is BRN alone (1.8×10^{-6} mol/L) at pH = 7.40 and 297 K.

2.11. Competitive binding site measurements

In presence of site markers (warfarin, ibuprofen and digitoxin), fluorescence measurements were performed for BSA-BRN system at pH = 7.40 and 297 K. The concentrations of BRN varied from 0 to 3.0×10^{-6} mol/L while both BSA and site markers concentrations were kept constant at 1.8×10^{-6} mol/L.

2.12. Influence of ions

BSA with Cu^{2+} , Ca^{2+} , Fe^{2+} , Mg^{2+} and Zn^{2+} ions were recorded for fluorescence spectra upon BRN addition at various concentrations of at 297 K and $\lambda_{\text{ex}} = 295$ nm. BSA and ions concentrations were put up constant at 1.8×10^{-6} mol/L and BRN various as 0 to 3.0×10^{-6} mol/L.

2.13. Statistical analysis

Triplicate measurements were made on all the conducted experiments; wherever applicable, mean values as well as standard deviations were estimated. OriginPro 9.0 software and Microsoft Excel were utilized for the interpretation of secured results.

3. Results and discussion

3.1. UV-visible absorption studies

UV-Vis absorption spectrum of BSA with various concentrations of BRN (Figure 2 (A)) exhibits the two absorption peaks strong one about 215 nm and weak one about 277 nm. The absorption peaks around 190-240 nm driven from $n \rightarrow \pi^*$ transitions of amide group which reflected the conformation of BSA [12]. Moreover, the bands around 190-240 nm increased with increasing concentrations of BRN by showing a spectral shift to higher wavelengths. This recommends that secondary structural modification occurred for BSA. A blue shift around 277 nm is typically identifies the changed polarity in micro-environments of Tyr and Trp ($\pi \rightarrow \pi^*$ transitions), which were considered as a sign of alteration in the BSA tertiary structure. Thus, BRN interacted with BSA by forming the complex. Also, BRN was induced conformational changes in BSA.

3.2. Fluorescence quenching mechanism

Tryptophan (two are Trp-134 and Trp-212) present in BSA (Figure 2 (B)) are affected by adding of BRN different concentrations that are revealed by momentous changes in emission fluorescence intensity at 334 nm (excitation was 295 nm). This suggested that BRN was interacted with BSA and faint red shift of fluorescence emission intimates increased hydrophobicity of Trp residues around its microenvironment.

By fluorescence spectral measurements at different temperatures (287, 297 and 307 K), three types of quenching mechanisms namely dynamic, static and combined static and dynamic were differentiated for BSA-BRN system [13]. The acquired data were examined through Stern-Volmer Equation (2) [14]

Table 1. Quenching constants (Stern-Volmer, rate and effective static) at various temperatures for BSA-BRN system *.

Compound	Temperature (K)	K_{SV} (L/mol) $\times 10^5$	k_q (L/mol.s) $\times 10^{13}$	K_a (L/mol) $\times 10^5$
BSA-BRN	287	3.44 \pm 0.07	12.74 \pm 0.02	5.53 \pm 0.06
	297	2.94 \pm 0.08	10.09 \pm 0.05	4.31 \pm 0.05
	307	2.39 \pm 0.02	8.85 \pm 0.04	1.86 \pm 0.08

* K_{SV} is Stern-Volmer quenching constant, k_q is quenching rate constant and K_a is effective static quenching constant.

Table 2. Thermodynamic and binding parameters for BSA-BRN interaction at discrete temperatures *.

Compound	Temperature(K)	K_b (L/mol) $\times 10^5$	n	ΔG (kJ/mol)	ΔH (kJ/mol)	ΔS (J/mol.K)
BSA-BRN	287	17.26 \pm 0.02	1.355 \pm 0.02	-34.54 \pm 0.03	-96.86 \pm 0.05	-217.16 \pm 0.04
	297	9.59 \pm 0.08	1.264 \pm 0.05	-32.36 \pm 0.07		
	307	1.33 \pm 0.06	1.070 \pm 0.06	-30.19 \pm 0.01		

* K_b is binding constant, n is number of binding sites, ΔG is change in Gibbs free energy, ΔH is change in enthalpy and ΔS is change in entropy.

Table 3. FT-IR spectral locations of free BSA and BSA-BRN complex at 297 K.

System	Amide I (cm ⁻¹)					Amide II (cm ⁻¹)
	1615-1637	1638-1648	1649-1660	1660-1680	1680-1692	
Free BSA	1623 \pm 0.28	1642 \pm 0.78	1652 \pm 0.57	1676 \pm 0.85	1687 \pm 0.81	1554 \pm 0.89
BSA-BRN	1629 \pm 0.52	1643 \pm 0.37	1651 \pm 0.62	1675 \pm 0.14	1682 \pm 0.59	1545 \pm 0.36

$$F_0 / F = 1 + k_q \tau_0 [Q] = 1 + K_{SV} [Q] \quad (2)$$

$$k_q = K_{SV} / \tau_0 \quad (3)$$

where, k_q and K_{SV} are the bimolecular and Stern-Volmer quenching constants, respectively. τ_0 and $[Q]$ are lifetime of Trp ($\sim 2.7 \times 10^{-9}$ s) present in free BSA without BRN and concentration of BRN, respectively. F_0 and F are BSA fluorescence intensities of in BRN absence and presence.

From Table 1 (Figure S1A), the computed k_q values are greater than 2.0×10^{10} L/mol.s (limiting diffusion rate constant) [15] and K_{SV} values decreases with increasing temperatures. Therefore, probable BRN quenching mechanism with BSA was static due to formed ground-state complex. Furthermore, a modified Stern-Volmer Equation (4) was applied to BSA-BRN system because not all fluorophores in BSA are evenly accessible to quencher (BRN); some portion of the fluorophores may not be impressed by quenchers, [16]

$$F_0 / (F_0 - F) = (1 / f_a) + (1 / K_a f_a [Q]) \quad (4)$$

where, f_a and K_a are the accessible segment of fluorophore and effective static quenching constant, respectively. Figure S1B represents the modified Stern-Volmer plot and their respective calculated values are enumerated in Table 1. Since, the measured K_a values diminished with increase of temperatures further confirming the quenching mechanism through static.

3.3. Binding parameters

Equation (5) [17] was employed to accompanying binding parameters namely n (binding sites in numbers) and K_b (binding constant) for static quenching inferred in BSA-BRN system.

$$\log[(F_0 - F) / F] = \log K_b + n \log [Q] \quad (5)$$

The ordinate and slope of $\log[(F_0 - F) / F]$ resistant to $\log [Q]$ were $\log K_b$ and n , respectively (Figure S1C). Table 2 demonstrates the estimations of K_b and n , and it could be noticed that K_b and n were diminished with the rising of temperature which were as per the pattern of quenching parameters as said above. This may represents that the formed BSA-BRN complex was unstable at higher temperatures by partly undergo decomposition. Even more, the n esteems were roughly equivalent to 1 implies that just a single BRN ties to BSA.

3.4. Binding forces estimated by thermodynamic parameters

Change in free energy (ΔG), enthalpy (ΔH) and entropy (ΔS) are thermodynamic variables were estimated for BSA-BRN system to the identification of binding forces involved in it. Assorted binding forces are usually hydrophobic, electrostatic, hydrogen bonding Van der Waals etc. The correlation of variable thermodynamics and binding forces was already reported for interaction to ligand-protein [18]. ΔH and ΔS values were examined from plot of $\ln K_b$ against $1/T$ by exerting Van't Hoff Equation (6), respectively (Figure S1C inset).

$$\ln K_b = (-\Delta H / RT) + (\Delta S / R) \quad (6)$$

where, R and T are gas constant and temperature, respectively. Additionally, ΔG was determined from Equation (7). The evaluated thermodynamics were in Table 2 tabulates.

$$\Delta G = \Delta H - T\Delta S \quad (7)$$

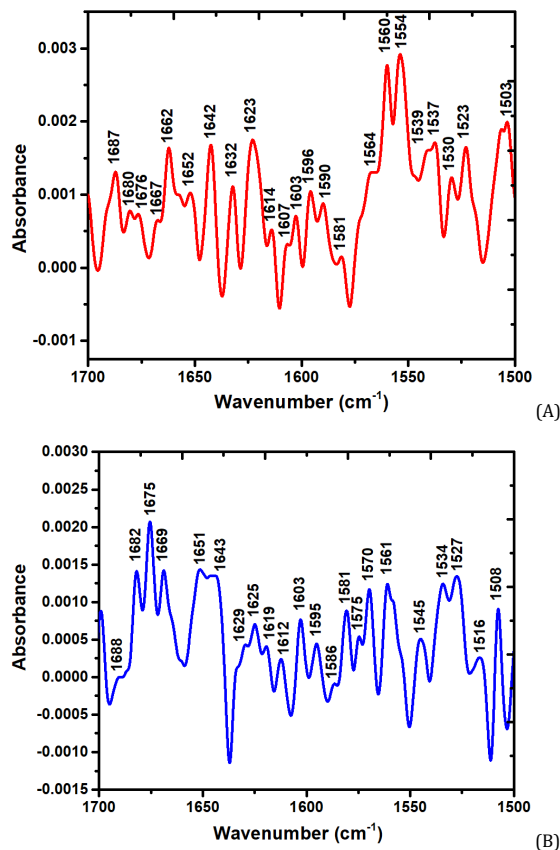
BSA and BRN interaction involves the spontaneous process, which was confirmed from the negative ΔG . Moreover, the negative ΔH and ΔS computed in this interaction point out to Van der Waals and hydrogen bonding forces, respectively. Also, ΔG is predominately entropy driven owing to higher value over to enthalpy. The obtained negative ΔH suggested the exothermic reaction.

3.5. Infrared measurements

As a great strategy, to find out secondary structures for proteins, infrared spectroscopy a long while been utilized. The peptide moieties among numerous amide bands in various vibrations are well displayed by proteins infrared spectra. Amide I band (1600-1700 cm⁻¹, stretching of C=O vibrations) most generally employed to examining protein secondary structures compare to amide II (1500-1600 cm⁻¹, coupled stretch and bend mode between C-N and N-H, respectively) due to sensitiveness and sub peaks are not mature [19]. The FT-IR spectra in amide I and II regions of BSA alone shows the shift in peak positions after undergo interaction with BRN which were characterized from Figure 3 and Table 3. More importantly, amide I band of BSA alone and BSA-BRN system was subjected to curve fitting methodology followed by secondary derivative with Fourier self-deconvolution for the estimation of secondary structural features (Figure 4) [20].

Table 4. Secondary structure estimations to free BSA and BSA-BRN complex by spectra of FT-IR and CD at 297 K.

Measurements	System	Secondary structures (%)				
		β -sheet	Random coil	α -Helix	β -Turn	β -Antiparallel
FT-IR	Free BSA	0.14±0.08	21.66±0.01	50.89±0.05	23.30±0.09	4.90±0.02
	BSA-BRN	1.99±0.07	20.82±0.04	41.88±0.04	24.74±0.05	10.57±0.07
CD	Free BSA	0.68±0.03	22.07±0.02	51.56±0.08	22.98±0.01	3.36±0.08
	BSA-BRN	2.15±0.06	19.27±0.05	42.91±0.09	25.69±0.04	9.98±0.02

**Figure 3.** FT-IR spectra: (A) BSA alone and (B) BRN bounded to BSA at 297 K. c (BSA) = c (BRN) = 6.0×10^{-6} mol/L.

Free BSA later binding with BRN, the components of α -helix and random coils reduced whereas β -sheet, β -antiparallel and β -turn increased (Table 4). Gathered charged and hydrophobic amino acids in the passage of the cavity forms the BRN binds to BSA at sub-domain IIA. The actual binding process may resulting from active functional arrays in BRN interacted with amino and prominent peptide chain of carbonyl groups. This generates secondary structural alterations caused by the transformation of carbonyl from polypeptide hydrogen bonding lattice work.

3.6. Circular dichroism studies

Figure 5 (A) shows CD spectrum to analyze the secondary structure of BSA with BRN interaction. α -Helical backbone structure of BSA was represented by two bands i.e., 209 and 222 nm at minima which were corresponding to transitions of $\pi \rightarrow \pi^*$ and $n \rightarrow \pi^*$, respectively [21]. After the addition of BRN, the CD spectral curve of BSA decreases, which demonstrating that the shapes of both the curves were similar but its ellipticity decreases. This signifies that the α -helix of free BSA decreased after interaction with BRN. The BRN absence and presence for BSA secondary structural calculations are presented in the Table 4. The altered BSA secondary structures were accomplished by increased β -antiparallel, β -sheet and β -turn with decreased random coils after interacted with BRN.

3.7. Fluorescence energy transfer by resonance

The distance separation of donor (BSA) and acceptor (BRN) was determined from FRET technique by applying Förster's theory [22]. FRET efficiency relies on distance of order 2-8 nm, orientation of transition dipole and overlap of fluorescence (BSA) with absorption (BRN). Energy transfer efficiency (E) between BSA and BRN is related to the distance (r) and critical energy transfer distance (R) is given by

$$E = R_0^6 / (R_0^6 + r^6) = (F_0 - F) / F_0 \quad (8)$$

$$R_0^6 = 8.8 \times 10^{-25} K^2 N^{-4} \Phi J \quad (9)$$

where, F_0 and F are the BSA fluorescence intensities at BRN absence and presence, respectively. K^2 , N and Φ are the dipole special orientation factor (2/3), medium refractive index (1.336), BSA (0.15) fluorescence quantum yield, respectively. J is the overlapping integral of BSA emission fluorescence and BRN absorption spectrum, it can be calculated by utilizing the Equation (10)

$$J = \left\{ \sum [F_d(\lambda) \varepsilon_a(\lambda) \lambda^4 \Delta\lambda] \right\} / \left\{ \sum [F_d(\lambda) \Delta\lambda] \right\} \quad (10)$$

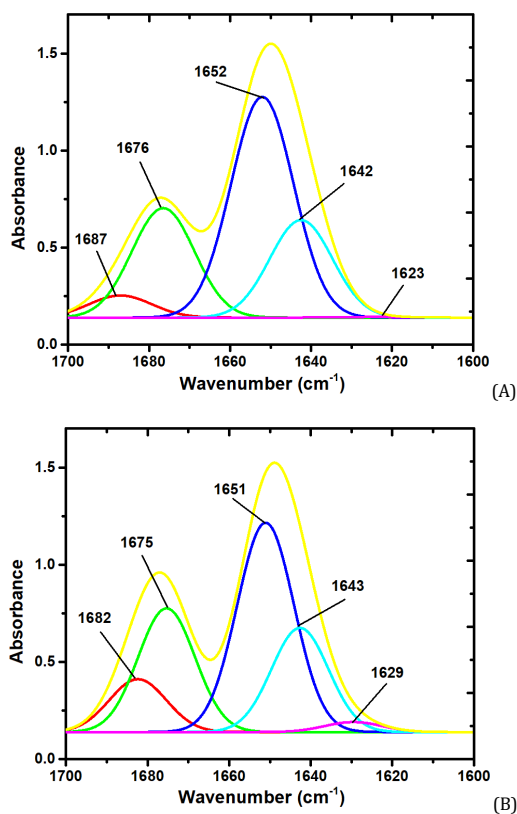


Figure 4. (A) Free BSA and (B) BSA-BRN system represented by curve fitting to amide I band at second derivative.

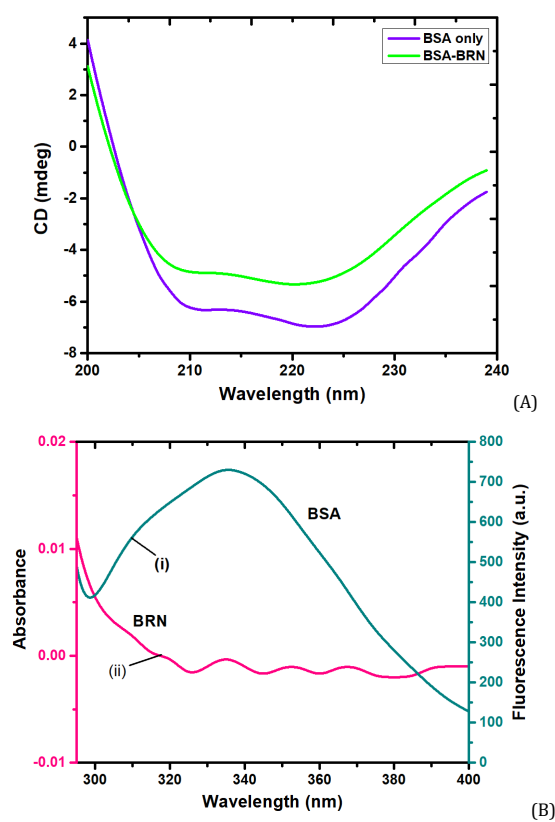


Figure 5. (A) CD spectra of BSA (6.0×10^{-6} mol/L) with and without BRN (120×10^{-6} mol/L) and (B) overlap of (i) fluorescence spectrum of BSA (6.0×10^{-6} mol/L) and (ii) UV-vis absorption spectrum of BRN (6.0×10^{-6} mol/L) at 297 K.

Table 5. Three binding sites characterization for BRN and BSA interaction by molecular docking.

Binding site	Interactions		Amino acid-BRN atom
	Type	Distance (Å)	
Site I (IIA)	Vander Waals	-	LEU218
		-	ARG217
		-	TRP213
		-	HIS241
		-	ILE289
		-	LEU259
		-	VAL240
		-	SER286
		-	ILE263
		-	ALA260
	Conventional Hydrogen Bond	2.04	ARG256:HE-O1
		2.01	ARG256:HH21-O1
	Pi-Sigma	3.96	LEU237:CD1-aromatic ring
3.61		LEU237:CD2-aromatic ring	
Alkyl	5.10	LYS221:(CB-CG-CD)-Cl1	
	4.31	ALA290:CB-Cl1	
Pi-Alkyl	4.11	ALA290:CB-aromatic ring	
Site II (IIIA)	Vander Waals	-	ARG409
		-	SER488
		-	TYR410
		-	ASN390
		-	ILE387
		-	THR448
		-	CYS391
		-	CYS436
		-	PHE394
		-	CYS437
		-	GLY433
		-	VAL432
		-	PHE402
		-	LEU406
	Alkyl	4.67	LEU386:(CD1-CG-CD2)- Cl1
Pi-Alkyl	5.12	LEU429:(CD2-CG-CD1)-aromatic ring	
	5.05	LEU452:(CD2-CG-CD1)-aromatic ring	
Site III (IB)	Vander Waals	-	LEU122
		-	GLU140
		-	PRO117
		-	TYR137
		-	ARG185
		-	ILE141
		-	ILE181MET184
	Amide-Pi Stacked	3.92	LYS136:(O=C=N)-aromatic ring
Pi-Alkyl	4.75	TYR160: aromatic ring-Cl1	
	3.38	PHE133: aromatic ring-Cl1	
	5.44	LEU115: (CD1-CG-CD2)-aromatic ring	

where, at λ , $F_d(\lambda)$ and $E_d(\lambda)$ are the BSA fluorescence intensity and BRN molar absorption coefficient, respectively. Overlapping spectrum of fluorescence emission of BSA (Trp134/Trp213) with absorption of BRN is represented by Figure 5 (B). The calculated $J = 8.47 \times 10^{-15} \text{ cm}^3\text{L/mol}$, $E = 35.0 \%$ and $R_0 = 0.239 \text{ \AA}$ values were assigned to found out $r = 0.264 \text{ \AA}$ value. The strong BSA and BRN binding and they are closest to each other was confirmed from r value. Moreover, the observed r was greater than R_0 further revealed that static quenching.

3.8. Molecular docking

The binding interaction between BRN and BSA was affirmed by *in silico* tests where the BRN was docked to BSA to foresee its mode of binding at the three major binding sites (Figure 6 and Table 5). In BSA: IIA called as site I, IIIA named as site II and IB as site III. Cluster analysis with binding energy for site I (79 modes and -30.12 kJ/mol), site II (24 modes, -18.22 kJ/mol) and site III (48 modes, -23.61 kJ/mol) revealed that BRN binds to BSA at site I (IIA) based on highest modes with lowest binding energy. Top ranked superior binding energy carried off for site I (Table S1) exhibiting $E_{\text{vdw+HB+desol}}$ very low value compared to E_{elec} and this representing that the main forces for BSA and BRN binding was hydrogen bond with Van der Waals. Further which was confirmed from more than

50% amino acids surrounds BRN were belonging to polar and ionic. Thus, suggested BRN binding at site I well agreed by experimental findings.

3.9. Synchronous fluorescence measurements

Synchronous fluorescence renders information on molecular environment of functional fluorophore group (Tyr and Trp) locality in proteins after interaction with fluorescence quencher. Allowing of simultaneous excitation with emission wavelengths scan, recorded this spectra. The variation in polarity at vicinity of fluorophore aromatic Tyr and Trp residues environment is achieved from the shift in the fluorescence emission peak position at maximum during quenching process. Shifts of red and blue signify the more environments of hydrophilic and hydrophobic, respectively. In synchronous fluorescence spectra, $\Delta\lambda$ at 15 and 60 nm values between excitation and emission wavelengths characteristics for Tyr and Trp residues, respectively [23]. This BSA intensity diminished with BRN increasing concentration (Figure 7 (B)) describes slight (~4 nm) red shift when $\Delta\lambda = 60 \text{ nm}$, whereas no shift was noticed for $\Delta\lambda = 15 \text{ nm}$ (Figure 7 (A)). Therefore, fluorescence quenching denotes that an interaction was occurred between BRN and BSA at vicinity of Trp by increased polarity. Also, BRN urges BSA conformational alterations.

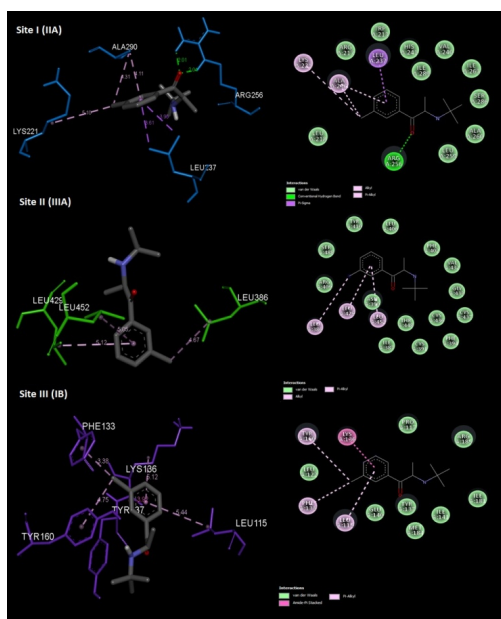


Figure 6. Three binding sites depiction to BSA-BRN system by molecular docking.

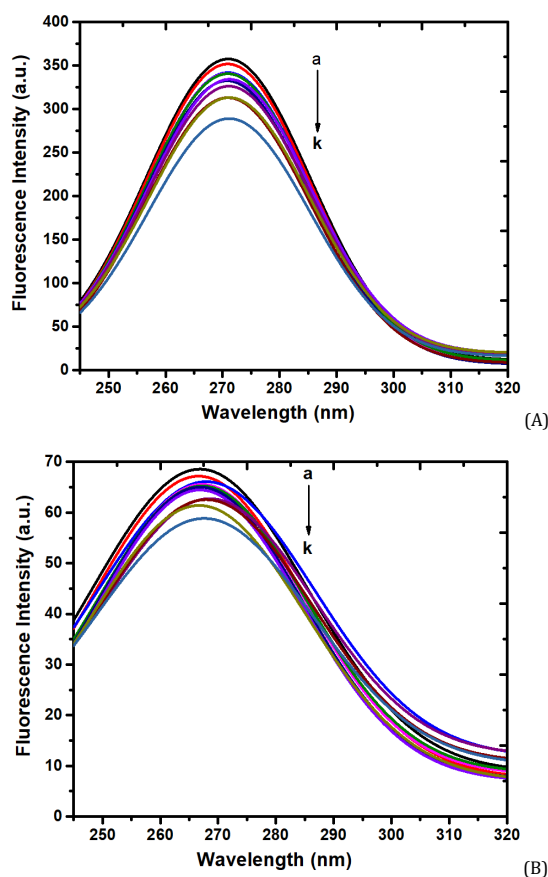


Figure 7. (A) $\Delta\lambda = 15$ nm and (B) $\Delta\lambda = 60$ nm: BSA (1.8×10^{-6} mol/L) synchronous fluorescence spectra by varying the amounts of BRN (0 to 3.0×10^{-6} mol/L) at 297 K.

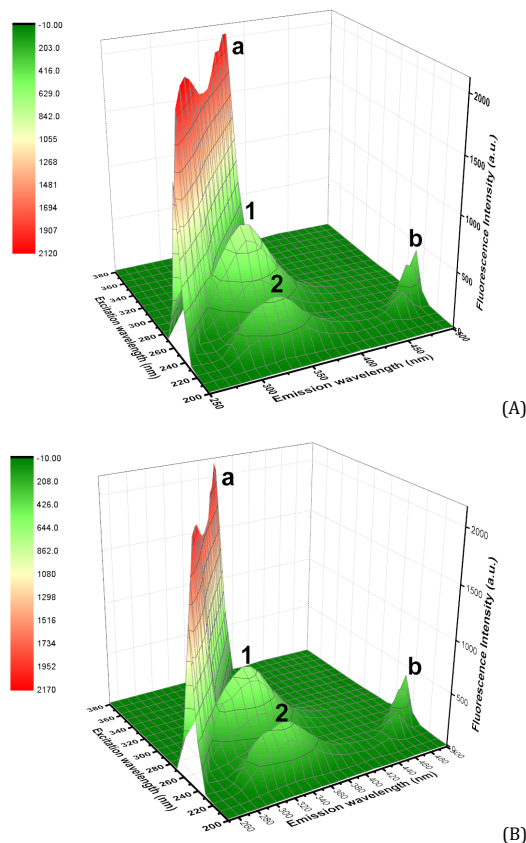
3.10. Three-dimensional fluorescence analysis

Figure 8 represents BSA spectra at 3D fluorescence in BRN absence and presence, which further determines the alteration in peptide backbone and microenvironment of Tyr/Trp residues. The observed spectral characteristics are in Table 6. Peak 'a' depicted Rayleigh scattering ($\lambda_{ex} = \lambda_{em}$) and 'b'

illustrating second-order scattering ($2\lambda_{ex} = \lambda_{em}$). Then again peak '1' portrays $n \rightarrow \pi^*$ transition of (Tyr and Trp) aromatic amino acids and '2' for $\pi \rightarrow \pi^*$ transition of peptide backbone [24]. All the peaks for BSA were reduced in BRN presence as could be noticed from the Figure 8 and Table 6. Hence, the microenvironment of Tyr/Trp residues and peptide backbone of BSA changed by forming BSA-BRN complex.

Table 6. Three-dimensional fluorescence illustrative to free BSA and BSA-BRN system at 297 K.

Peak position ($\lambda_{ex}/\lambda_{em}$, nm/nm)	Peak	Intensity	
		Free BSA	BSA-BRN
270/270→370/370	a	1971→2066	1864→2019
250/500	b	423.9	412.7
280/340	1	794.2	693.1
230/340	2	455.6	434.1

**Figure 8.** Fluorescence of 3D spectra: (A) free BSA and (B) BSA-BRN complex at 297 K. BSA to BRN concentration were 3.0×10^{-6} mol/L: 9.0×10^{-6} mol/L.

3.11. Identification of specific binding site on BSA for BRN

To find out the specific binding site of BRN on BSA was analyzed by using site markers. Sudlow *et al.* were confirmed that, warfarin, ibuprofen and digitoxin specifically bind to site I (IIA), site II (IIIA) and site III (IB) of BSA, respectively [25]. The fluorescence measurements were done to the system BSA-BRN system in the presence three site markers at pH = 7.40 and 297 K. Furthermore, the observed data were utilized for calculation of binding constants using Equation (5) by plotting the graph of $\log [(F_0 - F)/F]$ versus $\log [Q]$ (Figure S2A) and estimated K_b values are listed in the Table S2. K_b value for BSA-BRN system in warfarin presence of remarkably decreased whereas it remains unchanged for digitoxin and ibuprofen. This suggests that warfarin competes with BRN. Therefore BRN preferably binds to site I (IIA) on BSA.

3.12. Effects of metal ions

Blood system contains several metal ions which are not just play buffer action, osmotic pressure regulations and numerous physiological functions, yet in addition can straight forwardly influence the protein with drug interaction in terms of binding constant. The BSA-BRN complex in association with metal ions and their binding constants were evaluated from equation (5) (Table S2 and Figure S2B).

Except Ca^{2+} and Fe^{2+} , binding constant of BSA-BRN complex decreases, to be comparable with binding constant excluding these ions when the competition between BRN and the other ions occurred. Notwithstanding that, these ions and BRN are bind likely to BSA at different sites; they still inhibit binding between BRN and BSA. Consequently, drug to protein binding affinities could be weakened [26]. Ca^{2+} and Fe^{2+} ions induces the BSA alteration in conformation, which is more beneficial for BRN binding to BSA, on the other case via bridges of metal ion in BRN-metal ion complex bind more easily with BSA, these were the reason behind the increased binding constant [27] of BSA-BRN complex in presence Ca^{2+} and Fe^{2+} ions. Finally, shorten or elongation of the storage period of BRN in blood plasma affected by presence of common metal ions also improves or debilitates its most extreme impacts.

4. Conclusion

From experimental determinations, it was found that the hydrogen bonds and Van der Waals play key roles for BRN binding to BSA by undergoing efficient interaction through static quenching course of action at IIA sub-domain. Occurrence of energy transfer was achieved for distance r to BSA-BRN complex. Secondary structural contents and microenvironments altered for BSA upon BRN interaction. Metal Cu^{2+} , Ca^{2+} , Fe^{2+} , Mg^{2+} and Zn^{2+} ions affected the binding

process between BSA and BRN. This study is expected to afford some significant clues to the theoretical basis for pharmacology and clinical research.

Acknowledgements

Manjushree Makegowda raise their sincere esteems to University Grants Commission of Basic Scientific Research section (UGC-BSR) for awarding the fellowship under meritorious students, the CATERs CSIR-CLRI (Chennai, India) for CD spectral analysis and Institute Vijnana Bhavan, Mysuru for instrumental facilities.

Supporting information

The online version of this article contains supplementary material, which is available to authorized users.

Disclosure statement

Conflict of interests: The authors declare that they have no conflict of interest.

Author contributions: All authors contributed equally to this work.

Ethical approval: All ethical guidelines have been adhered.

Sample availability: Samples of the compounds are available from the author.

ORCID

Manjushree Makegowda

 <http://orcid.org/0000-0003-0298-4333>

Revanasiddappa Hosakere Doddarevanna

 <http://orcid.org/0000-0003-0127-3599>

References

[1]. Bupropion hydrochloride, RxList. <https://www.rxlist.com/wellbutrin-xl-drug.htm/>, 2018 (accessed 06 September 2018).

- [2]. Bupropion hydrochloride, WebMD. <https://www.webmd.com/drugs/2/drug-13507-7155/bupropion-hcl-oral/bupropion-extended-release-antidepressant-oral/details/>, 2018 (accessed 06 September 2018).
- [3]. Zhang, G.; Wang, L.; Fu, P.; Hu, M. *Spectrochim. Acta A* **2011**, *82*, 424-431.
- [4]. Zhang, Q.; Fu, X.; Garcia Martin, J. F. *Ultrason. Sonochem.* **2017**, *37*, 405-413.
- [5]. Manjushree, M.; Revanasiddappa, H. D. *J. Mol. Liq.* **2017**, *237*, 23-37.
- [6]. Sajid Ali, M.; Al-Lohedan, H. J. *Mol. Liq.* **2017**, *236*, 232-240.
- [7]. Skrt, M.; Benedik, E.; Podlipnik, C.; Ulrih, N. P. *J. Food. Chem.* **2012**, *135*, 2418-2424.
- [8]. Majorek, K. A.; Porebski, P. J.; A. Dayal, M. D.; Zimmerman, K.; Jablonska, A. J.; Stewart, M.; Chruszcz, W. *J. Mol. Immunol.* **2012**, *52*, 174-182.
- [9]. Ojha, B.; Das, G. *J. Phys. Chem.* **2010**, *114*, 3979-3986.
- [10]. Manjushree, M.; Revanasiddappa, H. D. *Spectrochim. Acta A* **2019**, *209*, 264-273.
- [11]. Lakowicz, J. R. *Principles of Fluorescence Spectroscopy*. Third ed. Springer, New York, 2006.
- [12]. Rosenheck, K.; Doty, P. *Proc. Natl. Acad. Sci. U. S. A.* **1961**, *47*, 1775-1785.
- [13]. Zhou, K.; Pan, D.; Lou, Y.; Shi, J. *J. Mol. Recognit.* **2018**, e2716.
- [14]. Sun, Z.; Xu, H.; Cao, Y.; Wang, F.; Mi, W. *J. Mol. Liq.* **2016**, *219*, 405-410.
- [15]. Lakowicz, J. R.; Weber, G. *Biochemistry* **1973**, *12*, 4161-4170.
- [16]. Chaves, O. A.; Silva, V. A.; Sant'Anna, C. M. R.; Ferreira, A. B. B.; Ribeiro, T. A. N.; Carvalho, M. G.; Cesarin-Sobrinho, D.; Netto-Ferreira, J. C. *J. Mol. Struct.* **2017**, *1128*, 606-611.
- [17]. Wei, X. L.; Xiao, J. B.; Wang, Y.; Bai, Y. *Spectrochim. Acta A* **2010**, *75*, 299-304.
- [18]. Ross, P. D.; Subramanian, S. *Biochemistry* **1981**, *20*, 3096-3102.
- [19]. Xi, J. Q.; Fan, L. *J. Therm. Anal. Calorim.* **2010**, *102*, 217-223.
- [20]. Katrahalli, U.; Jaldappagari, S.; Kalanur, S. *J. Lumin.* **2010**, *130*, 211-216.
- [21]. Yang, P.; Gao, F. *The Principle of Bioinorganic Chemistry*. Science Press: Beijing, China, 2002, pp. 349.
- [22]. Förster, T. *Delocalized excitation and excitation transfer*, O. Sinanoglu (Ed.), *Modern Quantum Chemistry. Istanbul Lectures 3*, Academic Press, New York/London, 1965, pp. 93-137.
- [23]. Zhang, Q.; Ni, Y.; Kokot, S. *J. Pharm. Biomed. Anal.* **2010**, *52*, 280-288.
- [24]. Molina-Bolívar, J. A.; Galisteo-González, F.; Ruiz, C. C.; Donnell, M. M.; Parra, A. *J. Mol. Liq.* **2015**, *208*, 304-313.
- [25]. Ni, Y.; Zhu, R.; Kokot, S. *Analyst* **2011**, *136*, 4794-4801.
- [26]. Wang, N.; Ye, L.; Yan, F.; Xu, R. *Int. J. Pharm.*, **2008**, *351*, 55-60.
- [27]. Xiao, J. B.; Chen, J. W.; Cao, H.; Ren, F. L.; Yang, C. S.; Chen, Y.; Xu, M. *J. Photochem. Photobiol. A* **2007**, *191*, 222-227.



Copyright © 2019 by Authors. This work is published and licensed by Atlanta Publishing House LLC, Atlanta, GA, USA. The full terms of this license are available at <http://www.eurjchem.com/index.php/eurjchem/pages/view/terms> and incorporate the Creative Commons Attribution-Non Commercial (CC BY NC) (International, v4.0) License (<http://creativecommons.org/licenses/by-nc/4.0>). By accessing the work, you hereby accept the Terms. This is an open access article distributed under the terms and conditions of the CC BY NC License, which permits unrestricted non-commercial use, distribution, and reproduction in any medium, provided the original work is properly cited without any further permission from Atlanta Publishing House LLC (European Journal of Chemistry). No use, distribution or reproduction is permitted which does not comply with these terms. Permissions for commercial use of this work beyond the scope of the License (<http://www.eurjchem.com/index.php/eurjchem/pages/view/terms>) are administered by Atlanta Publishing House LLC (European Journal of Chemistry).